International Journal of Solids and Structures 232 (2021) 111175

Contents lists available at ScienceDirect

International Journal of Solids and Structures

journal homepage: www.elsevier.com/locate/ijsolstr

A loaded beam in full frictionless contact with a couple stress elastic half-plane: Effects of non-standard contact conditions

E. Radi [a,b,*]

[a] Dipartimento di Scienze e Metodi dell'Ingegneria, Università di Modena e Reggio Emilia, 42122 Reggio Emilia, Italy
[b] Centro Interdipartimentale En&tech, Università di Modena e Reggio Emilia, 42122 Reggio Emilia, Italy

ARTICLE INFO

Article history:
Received 5 May 2021
Received in revised form 14 July 2021
Accepted 19 July 2021
Available online 24 July 2021

Keywords:
Contact problem
Euler-Bernoulli beam
Chebyshev polynomials
Green's function
Couple stress elasticity
Size effects

ABSTRACT

The plane problem of a loaded Euler-Bernoulli beam of finite length in frictionless bilateral contact with a microstructured half-plane modelled by the couple stress theory of elasticity is considered here. The study is aimed to investigate the size effects induced on the beam internal forces and moments by the contact pressure and couple stress tractions transmitted across the contact region. Use is made of the Green's functions for point force and point couple applied at the surface of the couple stress elastic half-plane. The problem is formulated by imposing compatibility of strain between the beam and the half-plane along the contact region and three alternative types of microstructural contact conditions, namely vanishing of couple stress tractions, vanishing of microrotations and compatibility between rotations of the beam cross sections and microrotations of the half-plane surface. The first two types of boundary conditions are usually assumed in the technical literature on micropolar materials, without any sound motivation, although the third boundary condition seems the most correct one. The problem is thus reduced to one or two (singular) integral equations for the unknown distributions of contact pressure and couple stress tractions, which are expanded in series of Chebyshev orthogonal polynomials displaying square-root singularity at the beam ends. By using a collocation method, the integral equations are reduced to a linear algebraic system of equations for the unknown coefficients of the series. The contact pressure and couple stress along the contact region and the shear force and bending moment along the beam are then calculated under various loading conditions applied to the beam, varying the flexural stiffness of the beam and the characteristic length of the elastic half-plane. The size effects due to the characteristic length of the half-plane and the implications of the generalized contact conditions are illustrated and discussed.

1. Introduction

Two-dimensional analyses of the contact problem of beams and plates resting on a deformable ground with microstructure are usually required in the field of micromechanics as well as in civil and biomechanical engineering, e.g. in the design of building foundations resting on granular materials, railway trucks laying on railway ballast and bone implants. For a preliminary analysis of the problem, the mechanical behaviors of the beam and ground are supposed to be elastic, in particular under serviceability conditions. If the support is made of inhomogeneous or granular material, like concrete, masonry, cellular materials and bones (Liu and Su, 2009; Eremeyev et al. 2016a; Eremeyev et al., 2016b; Eremeyev et al., 2017), then its constitutive relation may involve one or more characteristic lengths, defined by the sizes of the coarse and granular constituents. A similar situation occurs also for micro- and nanobeams supported by deformable layers, e.g. in MEMS and NEMS systems, where the size of the beam is comparable to the characteristic length associated to the materials inherent microstructure. In these cases, the mechanical response of the system may result as size dependent. Therefore, the classical theory of elasticity becomes inadequate and more enhanced constitutive theories are required for calculating the contact pressure accurately.

In order to predict the mechanical response of these components, an accurate investigation of the stress and strain fields arising along the contact region is mandatory, with special regard to stress concentration occurring at the edges, which can lead to loss of adhesion, debonding and other damaging phenomena affecting the durability and stability of the system.

* Address: Dipartimento di Scienze e Metodi dell'Ingegneria, Università di Modena e Reggio Emilia, 42122 Reggio Emilia, Italy.
E-mail addresses: enrico.radi@unimore.it, ~~eradi@libero.it~~

https://doi.org/10.1016/j.ijsolstr.2021.111175
0020-7683/

In order to circumvent some of the pathological results provided by the classical theory of elasticity, the use of enhanced constitutive models based on micropolar theories of elasticity has been proposed (Toupin, 1962, Mindlin and Tiersten, 1962, Mindlin, 1963). The simplest class of micropolar theories is represented by the indeterminate couple stress theory of elasticity, developed by Koiter (1964). This theory assumes that the microrotations are not independent but, rather, fully defined by the displacement field and actually coincident with the macroscopic rotations of the infinitesimal neighbourhood of the material point. Moreover, the local interaction between the continuum particles through a surface element occurs not only through a force vector, but also through a moment vector. Under plane strain conditions, this constitutive model features an additional material characteristic lengths, which allows to simulate the size effects.

Use of the indeterminate couple stress theory has been efficiently exploited in the analysis of stress concentration problems at the micro and nanoscale, such as in fracture mechanics of microstructured materials (Radi, 2007; Radi, 2008; Morini et al. 2013, Gourgiotis and Georgiadis, 2011; Nobili et al., 2019). Several investigations were recently performed on the contact problem between a rigid indenter of various shape and a couple stress elastic half-plane (Gourgiotis and Zisis, 2016; Gourgiotis et al., 2016; Karuriya and Bhandakkar, 2017; Song et al., 2017), thus neglecting the deformability of the indenter. In addition to the usual boundary conditions of the classic continuum, which constrain displacements and surface tractions, micropolar theories necessarily involve non-standard boundary conditions on the microrotation and micromoment. The works on the problem of indentation of a couple stress elastic materials usually assume that the moment tractions exchanged between the rigid indenter and the half-plane are equal to zero, even if these interactions can in principle be transmitted along the contact region. This choice is not necessarily justified from the physical point of view, but it is commonly assumed in order to recover the classical elastic solution as the characteristic length tends to zero. Such an assumption is also considered in the boundary conditions between a couple stress elastic material and a classical elastic material. For the plane problem of a circular inclusion in an infinite medium, Weitsman (1965) required continuity of displacements, rotation, tractions and couple stress tractions between the two materials modelled by using the couple stress theory of elasticity. As one of them tends to display classic elastic behavior, namely as the corresponding material length tends to zero, then it loses its substructure and the possibility of transmitting couple stress tractions.

In the analysis of a Mode III crack along the interface between couple-stress and classical elastic materials Piccolroaz et al. (2012) considered two types of transmission conditions. In the first case, these authors assumed that the couple-stress tractions are continuous at the interface, and thus vanishing. In the second case, they assumed instead that the rotations are continuous at the interface. It turns out that the solutions are quite different in the two cases and it is not possible to satisfy simultaneously both type of transmission conditions, so that a mismatch is always present at the interface, resulting either in a non-balanced couple-stress or a discontinuity in the micro-rotations.

Differently from the classical elastic continuum, an Euler-Bernoulli (EB) beam can instead transmit distributed couples when is put in contact with a micropolar material.

To our knowledge, the only attempts to enhance the classic contact conditions in the context of a micropolar continuum are the works of Zhang et al. (2005) and Lewandowski-Szewczyk and Stupkiewicz (2020). The former work proposed that the increment of the micromoment at the contact zone is proportional to the increment of the relative microrotation, with the proportionality coefficient depending on the contact pressure. The microblock contact model proposed in latter work assumes instead the coupling between the displacements and microrotations along the contact zone, as it follows from simple micromechanical considerations.

Investigations of the contact problem between an elastic beam and an elastic half-plane were performed by Shield and Kim (1992) by considering an EB beam welded to a classical elastic half-plane subject to a thermal mismatch strain. These Authors expressed the contact stresses through a series of orthogonal Chebyshev polynomials displaying square root singularity at the beam edges. Then, they found the series coefficient after the imposition of the strain compatibility condition along the contact zone by using a numerical collocation procedure. The analysis was also extended to the problem of a shear deformable beam in contact with a classical elastic half-plane by Lanzoni and Radi (2016) and to the beam buckling problem by Falope et al. (2020).

In the present work, the problem of a deformable EB beam of finite length in bilateral frictionless contact with a couple stress elastic half-plane is investigated by assuming that both contact pressure and couple stress tractions are transmitted across the contact zone. The couple stress theory of elasticity necessarily requires boundary conditions on the rotation and couple stress tractions in addition to the usual boundary conditions of the classic non-polar continuum on displacements and stress tractions. A challenging problem addressed in this work is thus how to extend the classic contact conditions to include the effects of the rotation and couple stress tractions. In the proposed approach, the classical strain compatibility condition between the slope of the beam and that of the half-plane surface is imposed along the contact region. Moreover, three types of microstructural contact conditions are considered and discussed, namely, vanishing of couple stress tractions, vanishing of rotations and compatibility between rotations of the half-plane surface and slope of the beam. The three alternative conditions lead to significantly different results in term of bending moment and shear force along the beam. By using the results of the asymptotic analysis performed by Gourgiotis and Georgiadis (2011) for Mode I crack-tip fields, both the contact pressure and couple stress tractions are assumed to display a square root singularity at the edges of the contact region. Then, they are expanded in series of orthogonal Chebyshev polynomials of the first kind. This assumption allows to remove the singularity of the integral equations. By means of a collocation technique, the problem is reduced to a linear algebraic system of equations for the unknown coefficients of the Chebyshev series expansion adopted for the contact pressure and couple stress tractions. The study allows to investigate the distribution of contact pressure and couple stress tractions along the contact region, varying the relative bending stiffness of the beam with respect to the elastic modulus of the half-plane and the ratio between the half-plane characteristic length and the beam length. Therefore, the present study represents an extension of the works on beams in contact with an elastic half-plane performed by Shield and Kim (1992), Lanzoni and Radi (2016), and those on rigid indentation of a couple stress elastic half-plane performed by Gourgiotis and Zisis (2016) and Zisis et al. (2018).

The paper is organized as follows. The governing equations for the EB beam under general loading and the couple-stress half-plane are reported in Section 2 and the 2D problem is approached by using Fourier transforms. The solution to the problem of a concentrated couple applied at the surface of the couple-stress half-plane is presented in Section 3 for the first time, together with some results obtained by Gourgiotis and Zisis (2016) and Zisis et al. (2018) for the problem of a concentrated force applied at the surface of the couple-stress half plane. The contact conditions between the beam and the half-plane surface are imposed in Section 4. The main results in terms of contact pressure, couple stresses tractions, bending moment and shear force along the beam are

reported in Section 5 for some relevant symmetric as well as skew-symmetric loading cases. Finally, conclusions are drawn in Section 6.

In this work, we concentrate on the size effects induced by the material characteristic length and on the proper definition of consistent non-standard contact conditions. For the sake of simplicity, we assume a bilateral frictionless contact. The associated unilateral contact problem will be considered in a forthcoming paper.

2. Governing equations

Let us consider an elastic EB beam of length $2a$ in bilateral frictionless contact with a couple stress elastic half-plane. The beam has arbitrary but uniform cross section of inertia moment I per unit width and Young modulus E_0, and is subjected to general transversal loading, denoted by $q(x)$, where $(0, x, y)$ is a Cartesian reference system with the x-axis aligned with the centroidal axis of the beam, ranging between $-a$ and a, and the y-axis directed towards the underlying half-plane, as shown in Fig. 1a. The balance equations of the beam then read:

$$T'(x) + q(x) - p(x) = 0, \quad M'(x) - T(x) + m(x) = 0, \tag{2.1}$$

where T and M are the internal shear force and bending moment along the beam, p and m denote the contact pressure and couple stress tractions transmitted between the beam and the half plane, which are assumed positive if they are directed as in Fig. 1b, and prime denotes differentiation with respect to coordinate x, namely $(\dots)' = \partial(\dots)/\partial x$.

By using the constitutive relations and the compatibility conditions for the EB beam, the bending moment and shear force of the beam cross section at abscissa x are given by the following relations in terms of the derivatives of the transversal deflection of the beam $v(x)$

$$M(x) = -E_0 I\, v''(x), \quad T(x) = -E_0 I\, v'''(x) + m(x). \tag{2.2}$$

From $(2.1)_1$ and $(2.2)_3$, the governing equation of the beam in terms of transversal deflection becomes

$$E_0 I\, v''''(x) = q(x) - p(x) + m'(x). \tag{2.3}$$

The boundary conditions for the problem considered here require the vanishing of the bending moment and shear force at both the beam ends, namely

$$M(\pm a) = 0, \qquad T(\pm a) = 0, \tag{2.4}$$

Integrating eqn (2.3) by parts three times between $-a$ and x, and using the boundary conditions (2.4) one may find the slope of the deflected beam as

$$v'(x) = \frac{1}{2E_0 I}\int_{-a}^{x} \{[q(t) - p(t)](x-t) + 2\,m(t)\}(x-t)\,dt + v'(-a) \tag{2.5}$$

together with the balance conditions for the entire beam

$$\begin{aligned} &\int_{-a}^{a} [q(t) - p(t)]\,dt = 0, \\ &\int_{-a}^{a} \{[q(t) - p(t)]\,t - m(t)\}\,dt = 0, \end{aligned} \tag{2.6}$$

Let F denote the resultant of the external load applied to the beam and e the abscissa of the corresponding point of application (eccentricity), namely

$$F = \int_{-a}^{a} q(x)\,dx, \quad e = \frac{1}{F}\int_{-a}^{a} q(x)\,x\,dx. \tag{2.7}$$

Under plane strain condition, the 2D displacement field in the couple stress elastic half-plane is defined by the components $u_x(x, y)$ and $u_y(x, y)$. Correspondingly, the strain, rotation and curvature fields are given by

$$\varepsilon_{xx} = u_{x,x}, \quad \varepsilon_{yy} = u_{y,y}, \quad \varepsilon_{xy} = (u_{x,y} + u_{y,x})/2, \tag{2.8}$$

$$\omega_z = (u_{y,x} - u_{x,y})/2, \quad \kappa_{xz} = \omega_{z,x}, \quad \kappa_{yz} = \omega_{z,y}, \tag{2.9}$$

respectively, where the rotation ω_z is assumed positive if clockwise directed. Hereinafter, a subscript comma denotes partial differentiation, e.g. $u_{x,y} = \partial u_x/\partial y$. In the absence of body forces, the balance equation for the couple stress elastic half-plane are

$$\begin{aligned} &\sigma_{xx,x} + \sigma_{yx,y} = 0, \\ &\sigma_{xy,x} + \sigma_{yy,y} = 0, \\ &\sigma_{xy} - \sigma_{yx} + m_{xz,x} + m_{yz,y} = 0, \end{aligned} \tag{2.10}$$

where σ and $\boldsymbol{m}$ are the nonsymmetric stress tensor and the couple stress tensor, respectively. The constitutive behavior of the couple stress elastic material is defined by three parameters, namely the shear modulus μ, the Poisson ratio ν and the characteristic length ℓ, which occur in the following constitutive equations between stresses and strains under plane strain conditions

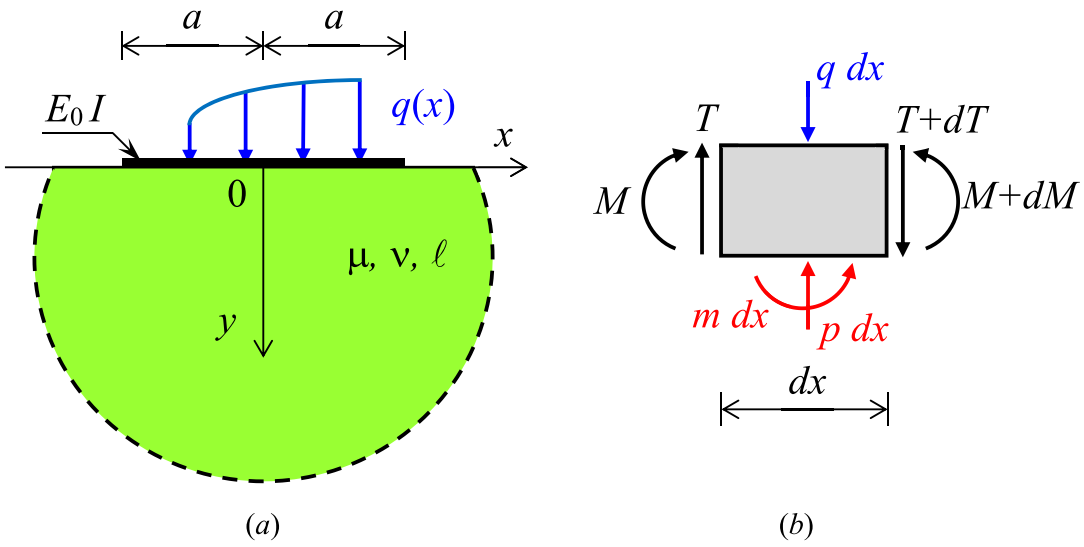

Fig. 1. Euler-Bernoulli beam of length $2a$ in bilateral frictionless contact with a couple stress elastic half-plane under general loading (a), and forces and couples acting on a very thin slice dx of beam.

$$
\begin{aligned}
2\mu\,\varepsilon_{xx} &= (1-\nu)\,\sigma_{xx} - \nu\,\sigma_{yy},\\
2\mu\,\varepsilon_{yy} &= (1-\nu)\,\sigma_{yy} - \nu\,\sigma_{xx},\\
4\mu\,\varepsilon_{xy} &= \sigma_{xy} + \sigma_{yx},
\end{aligned}
\tag{2.11}
$$

and between couple stresses and curvatures

$$
m_{xz} = 4\mu\ell^2\,\kappa_{xz}, \qquad m_{yz} = 4\mu\ell^2\,\kappa_{yz}. \tag{2.12}
$$

To satisfy the balance equations (2.10), the stress and couple stress components admit the following representation in terms of the Mindlin's stress functions $\Phi(x,y)$ and $\Psi(x,y)$ (Mindlin, 1963)

$$
\begin{aligned}
\sigma_{xx} &= \Phi_{,yy} - \Psi_{,xy},\\
\sigma_{yy} &= \Phi_{,xx} + \Psi_{,xy},\\
\sigma_{xy} &= -\Phi_{,xy} - \Psi_{,yy},\\
\sigma_{yx} &= -\Phi_{,xy} + \Psi_{,xx},
\end{aligned}
\tag{2.13}
$$

$$
m_{xz} = \Psi_{,x}, \qquad m_{yz} = \Psi_{,y}. \tag{2.14}
$$

According to (2.11) and (2.13), the strain fields can be written in terms of the two stress functions as

$$
\begin{aligned}
2\mu\,\varepsilon_{xx} &= \Phi_{,yy} + \Psi_{,xy} - \nu\,\Delta\Phi,\\
2\mu\,\varepsilon_{yy} &= \Phi_{,xx} + \Psi_{,xy} - \nu\,\Delta\Phi,\\
4\mu\,\varepsilon_{xy} &= -2\Phi_{,xy} + \Psi_{,xx} - \Psi_{,yy}
\end{aligned}
\tag{2.15}
$$

Moreover, the compatibility equations in term of stress yield the following differential relations between the two stress functions (Zisis et al., 2014; Zisis et al., 2018):

$$
\begin{aligned}
(\Psi - \ell^2\Delta\Psi)_{,x} + 2(1-\nu)\,\ell^2\Delta\Phi_{,y} &= 0,\\
(\Psi - \ell^2\Delta\Psi)_{,y} - 2(1-\nu)\,\ell^2\Delta\Phi_{,x} &= 0,
\end{aligned}
\tag{2.16}
$$

where Δ denotes the Laplace operator in the plane. Eqns (2.16) can be decoupled into the following two PDEs for the two stress functions

$$
\Delta\Delta\Phi = 0, \qquad \Delta\Psi - \ell^2\,\Delta\Delta\Psi = 0. \tag{2.17}
$$

In order to solve the boundary value problem considered here, the Fourier transform and its inverse are introduced. They are defined as follows

$$
\begin{aligned}
\bar{f}(s,y) &= \int_{-\infty}^{\infty} f(x,y)\,e^{isx}dx,\\
f(x,y) &= \frac{1}{2\pi}\int_{-\infty}^{\infty} \bar{f}(s,y)\,e^{-isx}ds,
\end{aligned}
\tag{2.18}
$$

where $i=(-1)^{1/2}$ is the imaginary unit. Therefore, the Fourier transforms of the governing equations (2.17) yield the following ordinary differential equations for the two stress functions

$$
\bar{\Phi}_{,yyyy} - 2s^2\,\bar{\Phi}_{,yy} + s^4\,\bar{\Phi} = 0, \tag{2.19}
$$

$$
\ell^2\,\bar{\Psi}_{,yyyy} - (1-2s^2\ell^2)\,\bar{\Psi}_{,yy} + s^2(1+s^2\ell^2)\,\bar{\Psi} = 0, \tag{2.20}
$$

which admit the following bounded solutions as $y\to\infty$:

$$
\bar{\Phi}(s,y) = [C_1(s) + y\,C_2(s)]\,e^{-|s|y}, \tag{2.21}
$$

$$
\bar{\Psi}(s,y) = C_3(s)\,e^{-|s|y} + C_4(s)\,e^{-\gamma y}, \tag{2.22}
$$

where $C_k(s)$ for $k=1,2,3,4$ are four unknown functions to be determined by using the boundary conditions at $y=0$, and

$$
\gamma = \sqrt{s^2 + 1/\ell^2}, \tag{2.23}
$$

According to the compatibility conditions $(2.16)_2$, the following relation holds between the functions $C_2(s)$ and $C_3(s)$

$$
C_3(s) = -4i(1-\nu)s\ell^2 C_2(s). \tag{2.24}
$$

The Fourier transforms of the stress and couple stress fields then become

$$
\begin{aligned}
\bar{\sigma}_{xx} &= \bar{\Phi}_{,yy} + is\,\bar{\Psi}_{,y},\\
\sigma_{yy} &= -s^2\,\bar{\Phi} - is\,\bar{\Psi}_{,y},\\
\bar{\sigma}_{yx} &= is\,\bar{\Phi}_{,y} - s^2\,\bar{\Psi},\\
\bar{\sigma}_{xy} &= is\,\bar{\Phi}_{,y} - \bar{\Psi}_{,yy},
\end{aligned}
\tag{2.25}
$$

$$
\bar{m}_{xz} = -is\,\bar{\Psi}, \qquad \bar{m}_{yz} = \bar{\Psi}_{,y}. \tag{2.26}
$$

Finally, the Fourier transforms of the displacement and rotation fields follow from the integration of the Fourier transforms of the strain fields as (Gourgiotis and Zisis, 2016; Zisis et al., 2018)

$$
\begin{aligned}
\bar{u}_x &= \frac{1}{2\mu}\left[\frac{1-\nu}{s}\,i\,\bar{\Phi}_{,yy} + i\nu s\,\bar{\Phi} - \bar{\Psi}_{,y}\right],\\
\bar{u}_y &= \frac{1}{2\mu}\left[\frac{1-\nu}{s^2}\,\bar{\Phi}_{,yyy} - (2-\nu)\,\bar{\Phi}_{,y} - is\,\bar{\Psi}\right],
\end{aligned}
\tag{2.27}
$$

$$
\bar{\omega}_z = \frac{1}{4\mu}\left[-\frac{2i}{s}(1-\nu)\left(\bar{\Phi}_{,yyy} - s^2\,\bar{\Phi}_{,y}\right) + \bar{\Psi}_{,yy} - s^2\,\bar{\Psi}\right], \tag{2.28}
$$

respectively.

3. Green's functions for the couple stress elastic half-plane

Let us first consider the boundary value problem of a clockwise couple C applied on the surface a couple stress elastic half-plane ($y>0$) at the origin of the coordinate reference system ($x=y=0$) (see Fig. 2). The intensity of the couple distributed along the out of plane direction is expressed in dimension of [force]. In this case, the boundary conditions along the surface $y=0$ are:

$$
\begin{aligned}
\sigma_{yy}(x,0) &= 0,\\
\sigma_{yx}(x,0) &= 0, \qquad \text{for} \quad -\infty < x < \infty,\\
m_{yz}(x,0) &= -C\,\delta(x),
\end{aligned}
\tag{3.1}
$$

where $\delta(x)$ is the Dirac delta function.

By using the representations of stresses and couple stresses (2.13) and (2.14) in terms of the stress functions, the Fourier transforms of the boundary conditions (3.1) then provide

$$
s\,\bar{\Phi}(s,0) + i\,\bar{\Psi}_{,y}(s,0) = 0,
$$

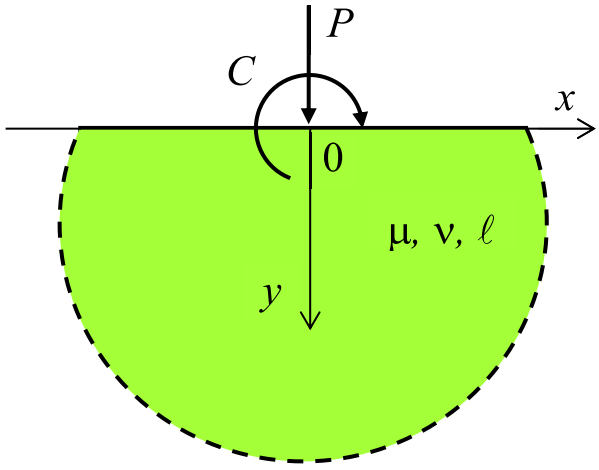

Fig. 2. Couple C and force P applied on the surface of a couple stress half-plane at the origin of the reference coordinate system.

$$i\,\bar{\Phi}_{,y}(s,0) - s\,\bar{\Psi}(s,0) = 0, \tag{3.2}$$

$$\bar{\Psi}_{,y}(s,0) = -C.$$

The introduction of (2.21) and (2.22) in Eq. (3.2), using also Eq. (24), then yields the following results for the unknown functions $C_i(s)$ for i = 1, 2, 3, 4:

$$\begin{aligned} C_1(s) &= \frac{i}{s}C, \\ C_2(s) &= i\,s\,\frac{\gamma - |s|}{|s|D(s)}\,C, \\ C_3(s) &= \frac{D(s) - \gamma}{|s|D(s)}C, \\ C_4(s) &= \frac{C}{D(s)}, \end{aligned} \tag{3.3}$$

where

$$D(s) = \gamma + 4(1-\nu)\,(\gamma - |s|)\,s^2\ell^2. \tag{3.4}$$

The substitution of the functions (3.3) into eqn (2.25)-(2.27) then provides the Fourier transforms of the stress, couple stress, and displacement fields. In particular, the Fourier transforms of the displacement components at the half-plane surface due to the couple C become

$$\begin{aligned} \bar{u}_x^C(s,0) &= \frac{1-\nu}{\mu}\frac{\gamma - |s|}{D(s)}\,C, \\ \bar{u}_y^C(s,0) &= i\,\frac{1-\nu}{\mu}\frac{s}{|s|}\frac{\gamma - |s|}{D(s)}\,C. \end{aligned} \tag{3.5}$$

Then, the inversion of Fourier transforms (3.5), according to $(2.18)_2$, yields

$$u_x^C(x,0) = C\,\frac{1-\nu}{\pi\,\mu}\int_0^\infty w(s\ell)\,\cos sx\,ds, \tag{3.6}$$

$$u_y^C(x,0) = C\,\frac{1-\nu}{\pi\,\mu}\int_0^\infty w(s\ell)\,\sin sx\,ds, \tag{3.7}$$

where

$$w(z) = \frac{\sqrt{1+z^2} - z}{\sqrt{1+z^2} + 4\,(1-\nu)(\sqrt{1+z^2} - z)\,z^2}. \tag{3.8}$$

Since $w(z) = O(z^{-2})$ as $z \to \infty$, then both displacement components (3.6) and (3.7) are vanishing at x = 0. The slope of the half-plane surface is given by

$$u_{y,x}^C(x,0) = C\,\frac{1-\nu}{\pi\,\mu}\int_0^\infty w(s\ell)\,s\,\cos sx\,ds. \tag{3.9}$$

The introduction of the stress functions (2.21) and (2.22) in (2.28), by using the results (3.3), and the successive inversion of the Fourier transforms then yield the rotation field at the half-plane surface due to the couple C applied at the origin of the Cartesian coordinate system

$$\omega_z^C(x,0) = C\,\frac{1-\nu}{\pi\,\mu}\int_0^\infty w(s\ell)\,\left[s + \frac{s+\gamma}{4(1-\nu)}\right]\cos sx\,ds. \tag{3.10}$$

The normalized variations of vertical displacement and rotation along the half-plane surface at y = 0, are plotted in Fig. 3 for three different values of the Poisson coefficient. It can be observed that the vertical displacement is vanishing at x = 0, whereas the slope and rotation display a logarithmic singularity as shown in the Appendix A. The Poisson coefficient has a noticeable influence on the vertical displacement, but it has a lower effect on the rotation field.

The Green's functions for the problem of a couple stress half-plane ($y \geq 0$) subject to a force P applied on its surface at the origin of the coordinate reference system ($x = y = 0$) (see Fig. 2) are derived in Gourgiotis and Zisis (2016) and Zisis et al. (2018) and some useful results are reported in the following. The intensity of the force distributed along the out of plane direction is expressed in dimension of [force][length]$^{-1}$, being distributed along the out of plane direction. In this case, the boundary conditions along the surface y = 0 are:

$$\begin{aligned} &\sigma_{yy}(x,0) = -P\,\delta(x), \\ &\sigma_{yx}(x,0) = 0, \quad \text{for} \quad -\infty < x < \infty. \\ &m_{yz}(x,0) = 0, \end{aligned} \tag{3.11}$$

By transforming these conditions and using eqn (2.24), the following solution for the unknown functions $C_k(s)$ (k = 1, 2, 3, 4) is obtained:

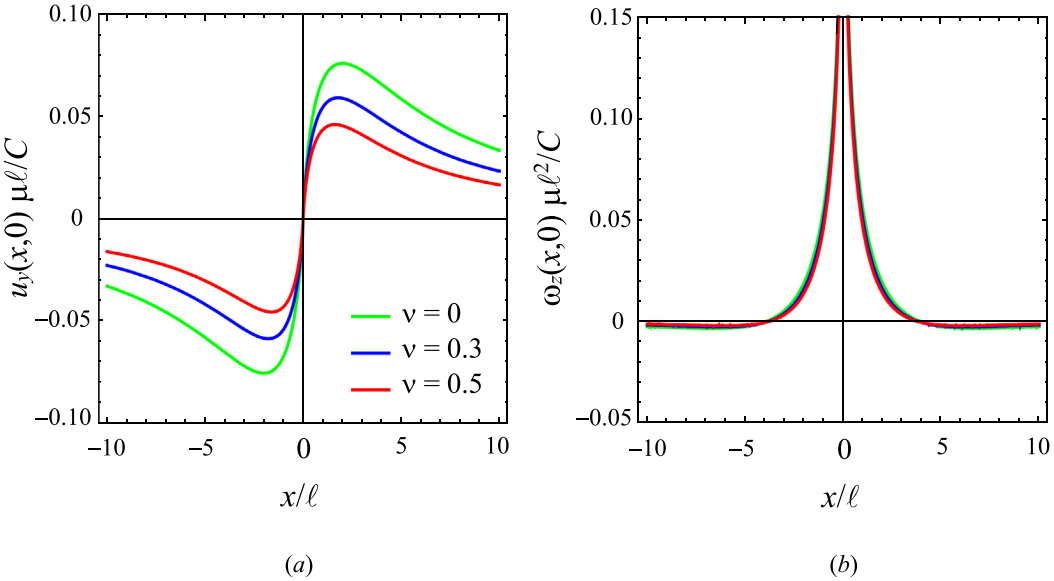

Fig. 3. Normalized variations of vertical displacement (a) and rotation (b) along the half-plane surface at y = 0, for three different values of the Poisson coefficient.

$$
\begin{aligned}
C_1(s) &= \frac{P}{s^2},\\
C_2(s) &= \frac{\gamma\, P}{|s| D(s)},\\
C_3(s) &= -4i\,(1-\nu)\, s\,\ell^2\,\frac{\gamma\, P}{|s| D(s)},\\
C_4(s) &= 4i\,(1-\nu)\, s\,\ell^2\,\frac{P}{D(s)},
\end{aligned}
\tag{3.12}
$$

where $D(s)$ is defined in (3.4). The corresponding slope along the surface of the couple stress elastic half-plane then is given by

$$
u^P_{y,x}(x,0) = \frac{P}{\pi\,\mu}\,\frac{1-\nu}{3-2\nu}\left[-\frac{1}{x} + 2(1-\nu)\int_0^\infty f(s\ell)\sin sx\; ds\right], \tag{3.13}
$$

where

$$
f(z) = \frac{2z^2(\sqrt{1+z^2}-z)-\sqrt{1+z^2}}{\sqrt{1+z^2}+4\,(1-\nu)(\sqrt{1+z^2}-z)\,z^2}, \tag{3.14}
$$

being $f(z) = O(z^{-2})$ as $z \to \infty$. The introduction of the stress functions (2.21) and (2.22) in (2.28), by using the results (3.12) and the successive inversion of the Fourier transform then yield the rotation field at the half-plane surface due to the force P

$$
\omega^P_z(x,0) = -\,P\,\frac{1-\nu}{\pi\,\mu}\int_0^\infty w(s\ell)\,\sin sx\; ds, \tag{3.15}
$$

whose trend is similar to the vertical displacement caused by a concentrated couple (3.7) plotted in Fig. 3a, which is vanishing at $x = 0$.

4. Contact conditions

Regarding the classical contact conditions between the EB beam and the couple stress half-plane, we assume vanishing shear stress as due to the frictionless assumptions and equal displacement of the beam and the half-plane surface along the normal direction. The former condition is met by the Green's functions derived in Section 3. The latter condition is better formulated in terms of slope, thus avoiding the introduction of a rigid body motion. Therefore, we impose that the slope of the beam is equal to the slope of the half-plane surface along the full length of the beam, namely

$$
v'(x) = u_{y,x}(x,\,0), \qquad \text{for } |x| \leqslant a, \tag{4.1}
$$

In eqns (4.1), the slope of the beam $v'(x)$ is given by (2.5), whereas the slope of the half-plane surface follows from the Green's functions (3.9) and (3.13) as

$$
\begin{aligned}
u_{y,x}(x,0) \;=\; & \frac{1-\nu}{\pi\,\mu}\left\{\frac{1}{3-2\nu}\int_{-a}^{a} p(t)\; dt\right.\\
& \times\left[-\frac{1}{x-t} + 2\,(1-\nu)\int_0^\infty f(s\ell)\,\sin[s\,(x-t)]\; ds\right]\\
& \left.+\int_{-a}^{a} m(t)\; dt\int_0^\infty w(s\ell)\; s\cos[s\,(x-t)]\; ds\right\}.
\end{aligned}
\tag{4.2}
$$

The admissible singularity for the stress and couple stress fields at the edge of the contact region are defined by the condition of vanishing tractions on the free surface and vanishing shear stress on the side of the beam contact. No conditions are imposed by eqn (2.3) on the higher order terms of contact pressure p and couple stress tractions m, due to the contribution of the higher order terms of the displacement fields provided by the term v''''. Therefore, the asymptotic fields in the half-plane near the beam edges must be similar to the Mode I crack-tip fields in couple stress elastic materials. According to the asymptotic analysis developed by Gourgiotis and Georgiadis (2011) for a Mode I crack problem, both the contact pressure $p(x)$ and the couple stress tractions $m(x)$ may display a square root singularity at both ends of the contact zone. Therefore, they can be assumed in the following form

$$
\begin{aligned}
p(x) &= \frac{F}{a}\sum_{n=0}^{\infty} p_n\,\frac{T_n(x/a)}{\sqrt{1-(x/a)^2}},\\
m(x) &= F\sum_{n=0}^{\infty} m_n\,\frac{T_n(x/a)}{\sqrt{1-(x/a)^2}},
\end{aligned}
\tag{4.3}
$$

for $|x| \leqslant a$, where p_n and m_n ($n = 0, 1, 2, \ldots$) are unknown coefficients, and T_n are the Chebyshev polynomials of order n of the first kind (see Appendix B). Note that the derivative of the couple stress tractions $m'(x)$, which appears in the governing equation (2.3), displays a singularity stronger than the contact pressure at the beam ends.

By using the result (B.2) provided in Appendix B, being $T_0(t) = 1$ and $T_1(t) = t$, the introduction of representations (4.3) and definitions (2.7) in the balance conditions (2.6) then provides the following two relations

$$
p_0 = \frac{1}{\pi}, \qquad m_0 = \frac{e}{\pi\,a} - \frac{p_1}{2}. \tag{4.4}
$$

The introduction of representations (4.3) and the following non-dimensional quantities

$$
\alpha \;=\; sa, \qquad \lambda = \ell/a, \tag{4.5}
$$

in eqns (2.5) and (4.2) then yields

$$
\begin{aligned}
v'(x) = v'(-a) + \frac{1}{2E_0 I}\left\{\int_{-1}^{x/a} q(t)(x-t)^2 dt\right.\\
\left.- Fa^2\sum_{n=0}^{\infty}\left[p_n A_n\left(\frac{x}{a}\right) - 2\; m_n\, B_n\left(\frac{x}{a}\right)\right]\right\},
\end{aligned}
\tag{4.6}
$$

$$
\begin{aligned}
u_{y,x}(x,\;0) \;=\; & F\frac{1-\nu}{\mu\,a}\left\{\frac{1}{3-2\nu}\sum_{n=0}^{\infty} p_n\left[U_{n-1}\left(\frac{x}{a}\right)\right.\right.\\
& \left.+ 2(1-\nu)\int_0^\infty f(\alpha\lambda)\, J_n(\alpha)\;\sin\left(\frac{\alpha x}{a} - \frac{n\pi}{2}\right) d\alpha\right]\\
& \left.+\sum_{n=0}^{\infty} m_n\int_0^\infty w(\alpha\lambda)\;\alpha\, J_n(\alpha)\cos\left(\frac{\alpha x}{a} - \frac{n\pi}{2}\right) d\alpha\right\},
\end{aligned}
\tag{4.7}
$$

where the results (B.3), (B.4) and (B.5) provided in Appendix B have been used, and the functions $A_n(\xi)$ and $B_n(\xi)$, for $n \geq 0$, are defined by

$$
\begin{aligned}
A_n(\xi) &= \int_{-1}^{\xi}\frac{T_n(\tau)}{\sqrt{1-\tau^2}}(\xi-\tau)^2 d\tau,\\
B_n(\xi) &= \int_{-1}^{\xi}\frac{T_n(\tau)}{\sqrt{1-\tau^2}}(\xi-\tau)\; d\tau.
\end{aligned}
\tag{4.8}
$$

Closed form expressions for the functions $A_n(\xi)$ and $B_n(\xi)$ are worked out in Appendix C.

The introduction of eqns (4.6) and (4.7) in the classical boundary condition (4.1) then yields the following relation for the unknown coefficients p_n and m_n (for $n \geq 1$) :

$$
\begin{aligned}
&\mu\frac{a}{F}\,v'(-a) + \frac{\beta}{2}\left\{\frac{a}{F}\int_{-1}^{\xi} q(a\tau)(\xi-\tau)^2 d\tau - \sum_{n=0}^{\infty}\left[p_n A_n(\xi) - 2\; m_n\, B_n(\xi)\right]\right\} =\\
&= \frac{1-\nu}{3-2\nu}\sum_{n=0}^{\infty} p_n\left[U_{n-1}(\xi) + 2\,(1-\nu)\int_0^\infty f(\alpha\lambda)\, J_n(\alpha)\,\sin\left(\alpha\xi - \frac{n\pi}{2}\right) d\alpha\right]\\
&+ (1-\nu)\sum_{n=0}^{\infty} m_n\int_0^\infty w(\alpha\lambda)\;\alpha\, J_n(\alpha)\cos\left(\alpha\xi - \frac{n\pi}{2}\right) d\alpha, \qquad \text{for } |\xi| \leqslant 1,
\end{aligned}
\tag{4.9}
$$

where $\xi = x/a$ and $\beta = \mu a^3/(E_0 I)$ are non-dimensional quantities, the latter denoting the relative bending compliance of the beam, namely the ratio between the elastic shear modulus of the half-

plane and the bending stiffness of the beam. The rotation of the cross section at the left end of the beam follows from eqn (4.9) for ξ = -1 as

$$\mu\frac{a}{F}\,v'(-a) = -\frac{1-v}{3-2v} \times \sum_{n=0}^{\infty} p_n \left[n(-1)^n + 2(1-v)\int_0^{\infty} f(\alpha\lambda)\,J_n(\alpha)\,\sin\left(\alpha+\frac{n\pi}{2}\right)d\alpha\right] + (1-v)\sum_{n=0}^{\infty} m_n \int_0^{\infty} w(\alpha\lambda)\,\alpha J_{n+1}(\alpha)\cos\left(\alpha+\frac{n\pi}{2}\right)d\alpha. \tag{4.10}$$

In the following, we consider three alternative types of microstructural contact conditions along the contact region, that can be added to the classical one (4.9).

4.1. Type I microstructural contact conditions

Vanishing of the generalized tractions on the contact surface is the simplest assumption and a common choice in contact mechanics of micropolar continua. Therefore, the first type of contact conditions assumes that no couple stress tractions are transmitted along the contact region, namely:

$$m(x) = 0, \qquad \text{for } |x| \leqslant a. \tag{4.11}$$

This assumption necessarily requires m_n = 0. In this case, the contact pressure coefficients p_n (for $n \geq 1$) are obtained from eqn (4.9) by using a collocation procedure and eqn (4.10) for $v'(a)$, as illustrated in Section 5.

4.2. Type II microstructural contact conditions

The second type of contact conditions assumes that rotations can not occur at the surface of the couple stress half-plane in frictionless contact with the beam, namely

$$\omega_z(x,\ 0) = 0, \qquad \text{for } |x| \leqslant a, \tag{4.12}$$

where the rotations $\omega_z(x, 0)$ at the surface of the half-plane follow from the Green's functions (3.10) and (3.15) as

$$\omega_z(x,0) = \frac{1-v}{\pi\mu}\left\{-\int_{-a}^{a} p(t)\,dt\int_0^{\infty} w(s\ell)\ \sin[s(x-t)]\,ds + \int_{-a}^{a} m(t)\,dt\int_0^{\infty} w(s\ell)\left[s+\frac{s+\gamma}{4(1-v)}\right]\cos[s(x-t)]\,ds\right\} \tag{4.13}$$

The introduction of representations (4.3) and non-dimensional quantities defined in (4.5) in eqn (4.13) then yields

$$\omega_z(x,\ 0) = F\frac{1-v}{\mu a}\sum_{n=0}^{\infty}\int_0^{\infty} w(\alpha\lambda)\,J_n(\alpha)\left\{m_n\left[\alpha+\frac{\alpha\lambda+\sqrt{1+(\alpha\lambda)^2}}{4\,(1-v)\,\lambda}\right] \times\cos\left(\frac{\alpha x}{a}-\frac{n\pi}{2}\right) - p_n\ \sin\left(\frac{\alpha x}{a}-\frac{n\pi}{2}\right)\right\}d\alpha \tag{4.14}$$

where the results (B.4) and (B.5) provided in Appendix B have been used. The introduction of eqn (4.14) in condition (4.12) then yields the following relation between the unknown coefficients p_n and m_n (for n = 1, 2, 3, ...):

$$\sum_{n=0}^{\infty}\int_0^{\infty} w(\alpha\lambda)\,J_n(\alpha)\left\{p_n\ \sin\left(\alpha\xi-\frac{n\pi}{2}\right) - m_n\left[\alpha+\frac{\alpha\lambda+\sqrt{1+(\alpha\lambda)^2}}{4(1-v)\,\lambda}\right]\cos\left(\alpha\xi-\frac{n\pi}{2}\right)\right\}d\alpha = 0. \tag{4.15}$$

In this case, the unknown coefficients p_n and m_n (for $n \geq 1$) follow from the system of equations (4.9) and (4.15) by using a collocation procedure, as shown in the next section.

4.3. Type III microstructural contact conditions

The first two types of boundary conditions are usually assumed in the technical literature on micropolar materials without any sound motivation. The last type of contact conditions considered here is more realistic. It assumes that the rotation at the surface of the couple stress half-plane in frictionless contact with the beam coincides with the slope of the beam, and thus with the rotation of the beam cross section, namely:

$$u_{y,x}(x,\ 0) = \omega_z(x,\ 0), \qquad \text{for } |x| \leqslant a. \tag{4.16}$$

In the undetermined theory of couple stress considered here, microrotations are indeed assumed to coincide with macrorotations and this condition has been exploited in formulating the contact conditions (4.16). As suggested by one of the reviewers, the boundary condition (4.16) is equivalent to the assumption of vanishing shear strain along the contact zone, namely ε_{xy} = 0 and thus $u_{x,y}$ = -$u_{y,x}$ for y = 0. Then, condition (4.16) follows from eqn $(2.9)_1$.

The introduction of eqns (4.7) and (4.14) in condition (4.16) then yields the following relation for the unknown coefficients p_n and m_n (for n = 1, 2, 3, ...):

$$\sum_{n=0}^{\infty}\left\{p_n\left[U_{n-1}(\xi)+\int_0^{\infty}\left(\frac{1}{3-2v}-\frac{\alpha\lambda}{d(\alpha\lambda)}\right)J_n(\alpha)\ \sin\left(\alpha\xi-\frac{n\pi}{2}\right)d\alpha\right] - \frac{m_n}{4(1-v)\ \lambda}\int_0^{\infty}\frac{J_n(\alpha)}{d(\alpha\lambda)}\cos\left(\alpha\xi-\frac{n\pi}{2}\right)d\alpha\right\} = 0. \tag{4.17}$$

for $|\xi| \leq 1$, where

$$d(z) = \sqrt{1+z^2} + 4\,(1-v)(\sqrt{1+z^2}-z)\,z^2. \tag{4.18}$$

In this case, the unknown coefficients p_n and m_n (for $n \geq 1$) follow from the system of two integral equations (4.9) and (4.17) by using a collocation procedure, as detailed in the next section.

It should be noted that the adoption of contact conditions on rotation in eqns (4.12) and (4.16) leads to an over-constrained version of the classical elasticity solution. In these two cases, the couple stress-based solution is not expected to approach to the classical elastic solutions as $\ell \to 0$ (Karuriya and Bhandakkar, 2017).

5. Numerical solution and results

If a finite number N of terms is considered in the series (4.3), then the compatibility condition (4.10) together with the considered microstructural contact condition defined in Section 4 are imposed at N properly selected collocation points x_k, being p_0 and m_0 known from the balance conditions (4.4). In the present case, the optimal collocation points are the roots of the Chebyshev polynomial $T_N(x)$, namely

$$x_k = \cos\left(\frac{2k-1}{2N}\,\pi\right), \qquad \text{for } k = 1,\ 2,\ \ldots, N. \tag{5.1}$$

The proposed approach allows to transform the system of one or two integral equations into a linear system of N or $2N$ algebraic equations, respectively, that can be solved for the unknown coefficients p_n and m_n, for n = 1, 2,..., N, introduced in (4.3). The regularity of this kind of algebraic system and the rate of convergence have been studied in detail (e.g. Erdogan, 1969; Erdogan, and Gupta, 1972).

Once the contact pressure and couple stress tractions under the beam are known, the distribution of bending moment and shear force along the beam can be obtained from eqns (2.2) and (2.5) namely:

$$M(x) = -\int_{-a}^{x} \{[q(t) - p(t)](x - t) + m(t)\}\, dt,$$
$$T(x) = -\int_{-a}^{x} [q(t) - p(t)]\, dt, \tag{5.2}$$

Then, the introduction of representations (4.3) for a finite number N of terms and definitions (2.7) in Eq. (5.2) yields

$$M(x) = Fa \sum_{n=0}^{N} \left[p_n B_n\left(\frac{x}{a}\right) - m_n C_n^{(0)}\left(\frac{x}{a}\right)\right] - \int_{-a}^{x} q(t)(x - t)\, dt, \tag{5.3}$$

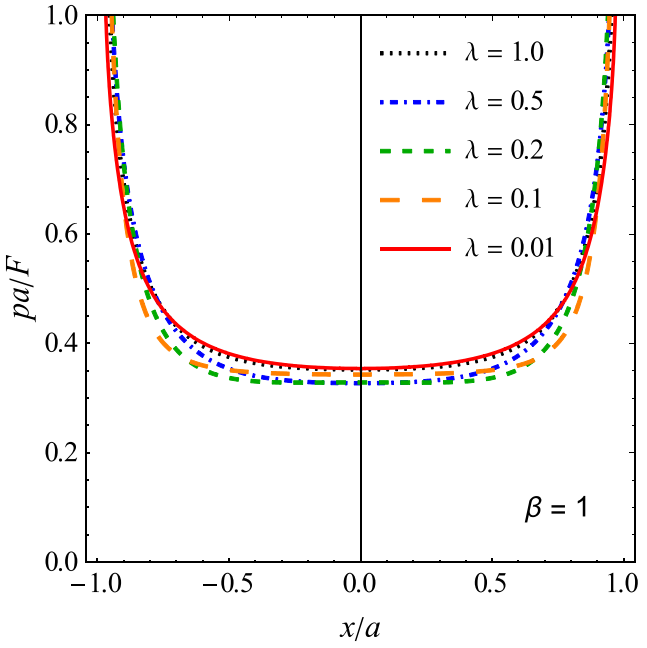

Fig. 4. Distributions of contact pressure under the beam due to a uniformly distributed loading $q = F/(2a)$, for $\beta = 1$ and $\nu = 0.3$, for some values of the non-dimensional ratio $\lambda = \ell/a$, for microstructural boundary conditions of Type I.

$$T(x) = F \sum_{n=0}^{N} p_n C_n^{(0)}\left(\frac{x}{a}\right) - \int_{-a}^{x} q(t)\, dt, \tag{5.4}$$

where B_n is defined in eqn (4.8) and calculated in Appendix C, and

$$C_n^{(0)}(\xi) = \int_{-1}^{\xi} \frac{T_n(\tau)}{\sqrt{1 - \tau^2}}\, d\tau, \tag{5.5}$$

whose closed form expression is provided in (C.2) in Appendix C.

The distributions of contact pressure and couple stress tractions under the beam are calculated for the three types of microstructural contact conditions considered in the previous sections, under uniformly distributed loading or concentrated load applied to the beam, varying the bending compliance of the beam and the characteristic length of the elastic half-plane through the parameters β and λ, respectively. All the results reported in the following are obtained for the Poisson coefficient $\nu = 0.3$ and for a number of terms N in the series larger than 30. Symmetric loading conditions are considered first. Under symmetric loading, the distribution of contact pressure p along the contact region is symmetric, whereas that of the couple stress tractions m is skew-symmetric.

The normalized distribution of contact pressure under the beam due to a uniformly distributed loading applied to the beam for vanishing couple stress tractions as required by type I microstructural contact conditions is reported in Fig. 4 for $\beta = 1$ and for some values of the non-dimensional ratio $\lambda = \ell/a \leq 1$. It can be observed that the contact pressure is everywhere compressive and displays a square-root singularity at both ends. The results for very small value of the characteristic length, e.g. for $\lambda = 0.01$, are expected to approach the classical elastic solution. It can be observed that the distributions for $\lambda = 1$ and $\lambda = 0.01$ are almost coincident, whereas the contact pressure for intermediate values of λ displays a slight reduction in the central zone and a corresponding increase near the beams ends. Therefore, the effects of the micropolar property of the ground are limited if contact conditions of Type I are assumed. The corresponding normalized distributions of bending moment and shear force along the beam are plotted in Fig. 5a and 5b. Again, the distributions for $\lambda = 1$ and $\lambda = 0.01$ are almost coincident, whereas the curves for intermediate values of λ display a noticeable increase in the maximum values.

Distributions similar to those reported in Figs. 4 and 5, but for microstructural contact conditions of type II, are plotted in Figs. 6

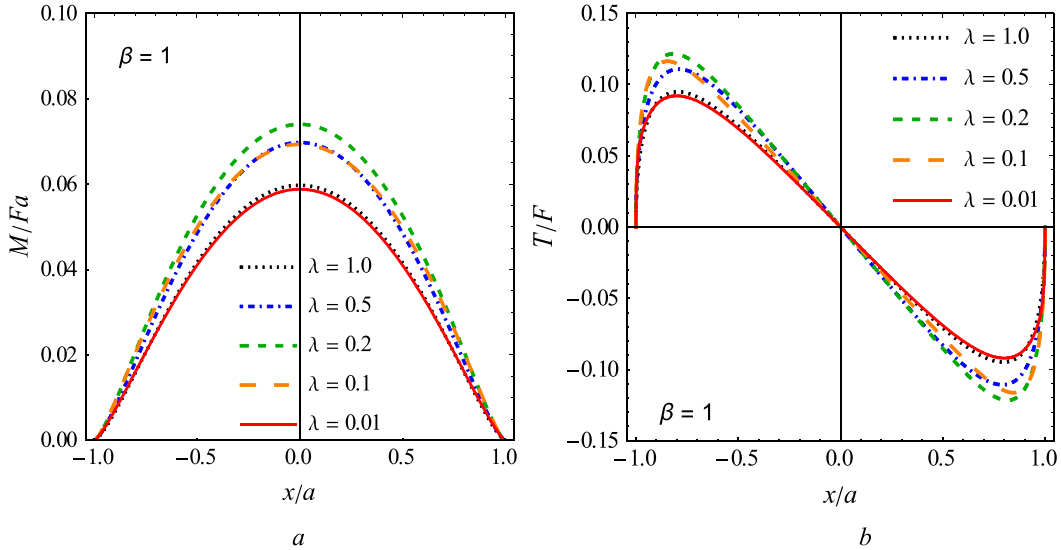

Fig. 5. Distributions of bending moment (a) and shear force (b) along the beam due to a uniformly distributed loading $q = F/(2a)$, for $\beta = 1$ and $\nu = 0.3$, for some values of the non-dimensional ratio $\lambda = \ell/a$, for microstructural boundary conditions of Type I.

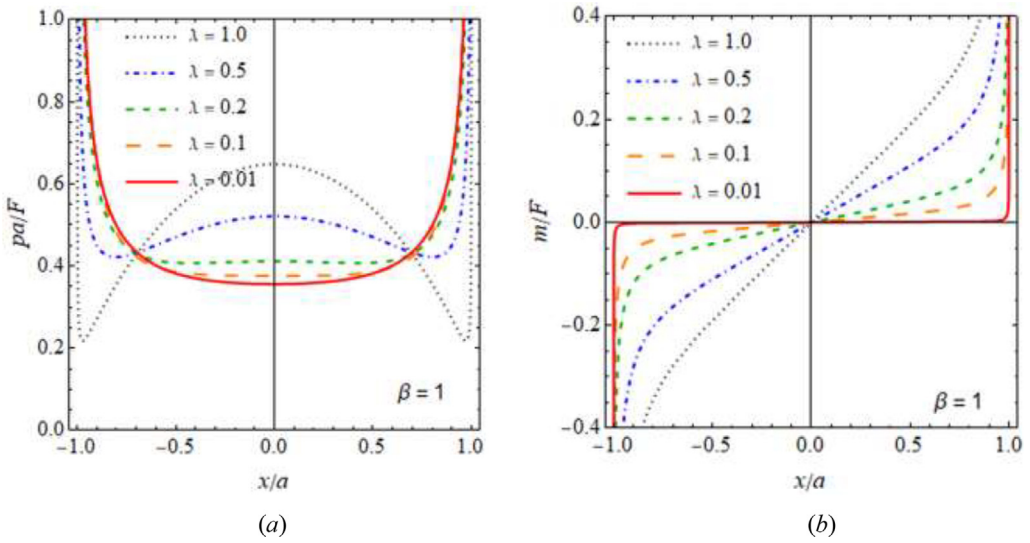

Fig. 6. Distributions of contact pressure (a) and couple stress tractions (b) under the beam due to a uniformly distributed loading $q = F/(2a)$, for $\beta = 1$ and $\nu = 0.3$, for some values of the non-dimensional ratio $\lambda = \ell/a$, for microstructural boundary conditions of Type II.

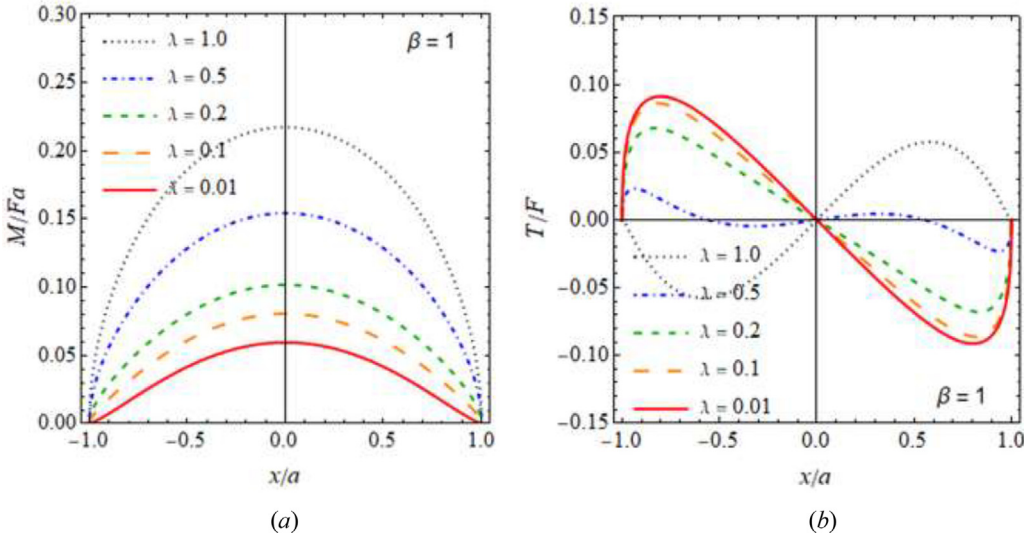

Fig. 7. Distributions of bending moment (a) and shear force (b) along the beam due to a uniformly distributed loading $q = F/(2a)$, for $\beta = 1$ and $\nu = 0.3$, for some values of the non-dimensional ratio $\lambda = \ell/a$, for microstructural boundary conditions of Type II.

and 7. In this case, the effect of the material characteristic length is more pronounced. As the characteristic length increases indeed, the distribution of contact pressure in Fig. 6a remarkably increases at the center of the contact zone and it decreases at the edges, where it is compressive and singular. Also the couple stress tractions in Fig. 6b remarkably increase with the characteristic length and display singular behavior at both ends. Note that for a very small characteristic length ($\lambda = 0.01$) the couple stress tractions vanishes almost everywhere in the contact region, except at the edges where they tend to concentrate.

The corresponding effects on the beam consist in a significant increase in the bending moment and a reduction in the shear force as the characteristic length increases, as plotted in Fig. 7a and 7b, respectively. In particular, for large values of the characteristic length, e.g. for $\lambda = 1$, the internal shear force displays the opposite sign along the beam length (dotted line in Fig. 7b). These effects are mainly due to the contribution of moment tractions, which are required for preventing the rotations at the half-plane surface, as required by the Type II microstructural contact conditions. This kind of contact conditions is almost unrealistic and its use may be questionable, specially for a frictionless contact problem, although the rotation of the element in contact can be constrained also if the interface is frictionless.

The distributions of contact pressure, couple stress tractions, bending moment and shear force along the beam under Type III microstructural contact conditions are then plotted in Figs. 8 and 9. In this case, the contact pressure is almost unaffected by the size of the material characteristic length (Fig. 8a), whereas the couple stress tractions within the contact region exhibit a non-monotonic trend as the characteristic length is increased. Namely, their magnitude increases up to $\lambda \approx 0.2$–0.3, and then it decreases and displays the opposite sign in the central part of the contact zone for larger values of λ (Fig. 8b). Correspondingly, the bending moment along the beam at first increases with the characteristic length and attains its maximum values at the center of the beam for $\lambda \approx 0.2$–0.3. Then, it decreases for larger values of λ. No significant effects of the characteristic length are instead observed on the shear force distribution, being the contact pressure also unaffected by its variation.

The proper choice of the contact conditions depends on the microstructural characteristic of the contact surfaces. A reasonable

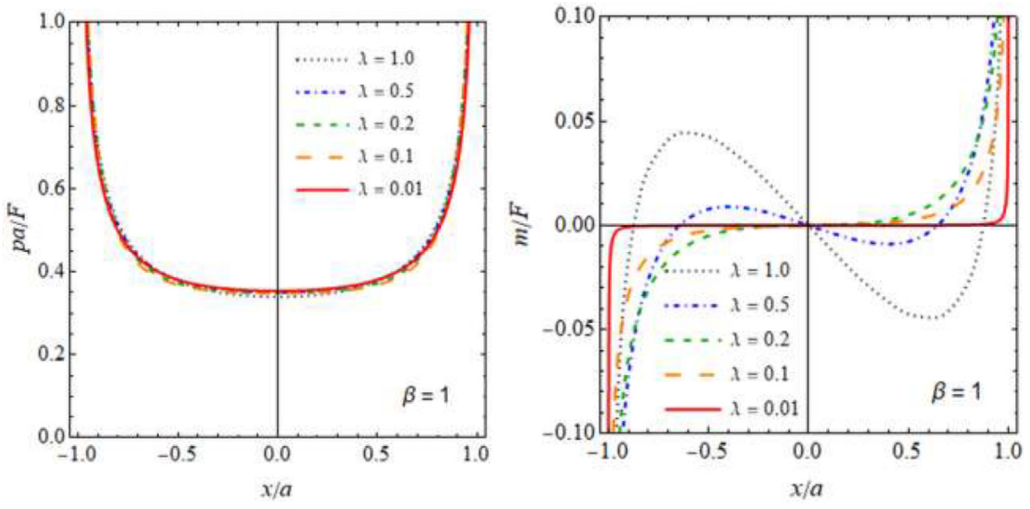

Fig. 8. Distributions of contact pressure (a) and couple stress tractions (b) under the beam due to a uniformly distributed loading $q = F/(2a)$, for $\beta = 1$ and $\nu = 0.3$, for some values of the non-dimensional ratio $\lambda = \ell/a$, for microstructural boundary conditions of Type III.

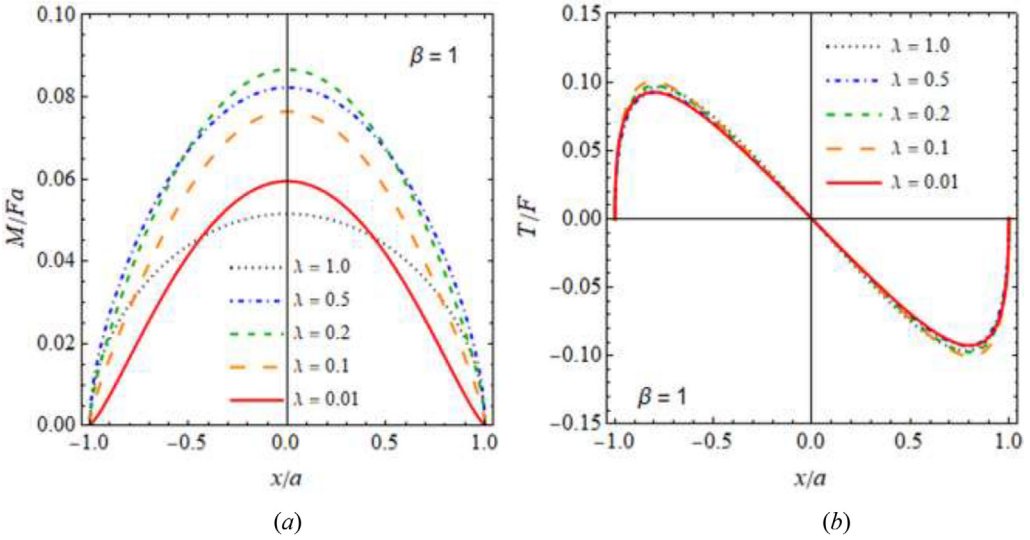

Fig. 9. Distributions of bending moment (a) and shear force (b) along the beam due to a uniformly distributed loading $q = F/(2a)$, for $\beta = 1$ and $\nu = 0.3$, for some values of the non-dimensional ratio $\lambda = \ell/a$, for microstructural boundary conditions of Type III.

assumption is represented by type III, which assumes coincidence between rotations of the half-plane surface and macroscopic rotations of the beam cross section.

A common feature observed for all the three types of contact conditions considered here is the evident size-effect on the magnitude of the bending moment predicted by the present solution in Fig. 5a, 7a and 9a when the beam length becomes comparable to the intrinsic characteristic length scale of the ground. The observed size-effect is particularly emphasized for contact conditions of Type II. In this case, the bending moment for $\lambda = 1$ in Fig. 7a is four times larger than that for vanishing small λ. Moreover, as the characteristic length becomes vanishing small, the couple stress tractions tend to vanish also for contact conditions of types II and III, and the contact pressure tends to the classical elastic solution.

The effects of the relative compliance of the beam β with respect to the ground on the distributions of contact pressure and internal bending moment and shear force have been highlighted in Figs. 10 and 11 for microstructural contact conditions of Type III, for $\lambda = 0.1$, under uniformly distributed loading. Note that low values of the non-dimensional parameter β denote high bending stiffness of the beam with respect to the ground. Conversely, high values of β denote compliant beams. The case of a plane rigid indenter can be recovered as the limiting case for $\beta = 0$. As the relative bending compliance β of the EB beam increases, the contact pressure increases at the center of the contact zone and decreases at the edges (Fig. 10a) and the couple stress tractions decreases and change sign in the central zone (Fig. 10b). Correspondingly, the magnitudes of both bending moment and shear force along the beam significantly decrease (Fig. 11), in agreement with the classical elastic solution (Shield and Kim, 1992; Sackfield et al., 2013; Barber, 2018).

A beam subject to a point force F applied at its midspan for microstructural contact conditions of Type III is then considered in Figs. 12 and 13, for $\beta = 1$, and for some values of the non-

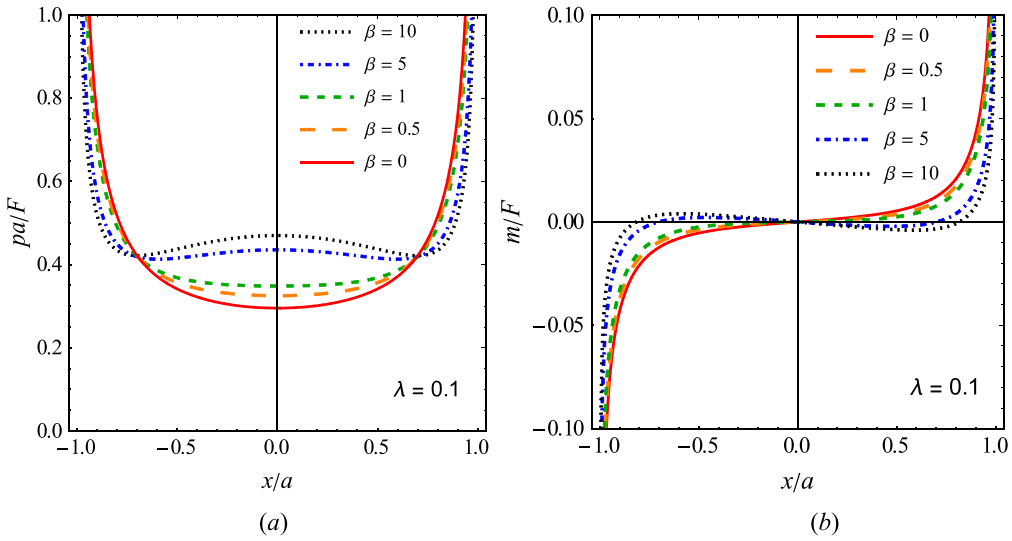

Fig. 10. Distributions of contact pressure (a) and couple stress tractions (b) under the beam due to a uniformly distributed loading $q = F/(2a)$, for $\lambda = 0.1$ and $\nu = 0.3$, for some values of the non-dimensional ratio β, for microstructural boundary conditions of Type III.

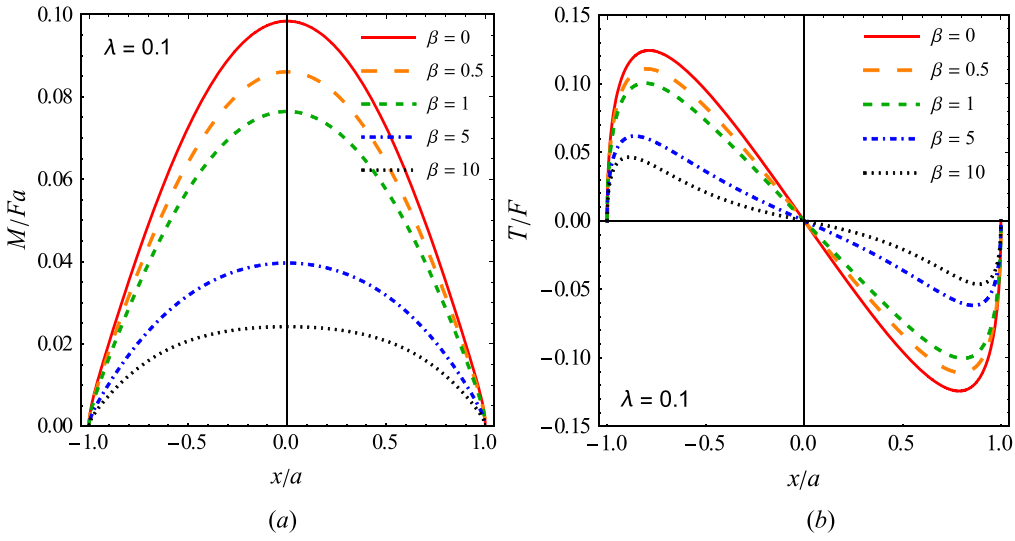

Fig. 11. Distributions of bending moment (a) and shear force (b) along the beam due to a uniformly distributed loading $q = F/(2a)$, for $\lambda = 0.1$ and $\nu = 0.3$, for some values of the non-dimensional ratio β, for microstructural boundary conditions of Type III.

dimensional ratio λ. For such a loading condition, the contact pressure displays a relative maximum under the point load (Fig. 12a) and it is only marginally affected by the size of the characteristic length of the ground. Conversely, the couple stress tractions display an opposite trend which grows up (in modulus) in the central part of the contact region as λ increases, as reported in Fig. 12b. Note that, due to symmetry, the couple stress tractions vanish at the middle of the beam whatever the parameter λ. Correspondingly, the bending moment along the beam plotted in Fig. 13a displays a sharp peak under the point load, whose value decreases only for large characteristic lengths, namely for $\lambda \geq 0.5$. The shear force plotted in Fig. 13b is discontinuous across the load application point, namely at $x = 0$ and it is almost unaffected by λ.

Finally, the contact pressure and the internal forces and moment due to a point force F applied at the beam with eccentricity $e = \delta\, a$ are reported in Figs. 14 and 15, for some values of δ, for microstructural contact conditions of Type III, for $\beta = 1$ and $\lambda = 0.1$. For such asymmetric loading condition, the normalized contact pressure plotted in Fig. 14a increases at the side of the load application (on the right) and it decreases at the opposite end (on the left), where it tends to vanish for δ a bit larger than 0.5. If the eccentricity of the load is further increased, then the contact pressure is expected to become tensile. In this case, debonding may occur if the beam is not sufficiently bonded to the ground. As δ increases, the couple stress tractions change sign at the edge far from the load application point and tend to assume the same sign all through the contact zone (Fig. 14b). The bending moment along the beam plotted in Fig. 15a displays a sharp peak just under the load application point, whose value decreases as the eccentricity increases. Correspondingly, the shear force plotted in Fig. 15b is discontinuous across the load application point, and its maximum magnitude displays a slight increase with the eccentricity δ.

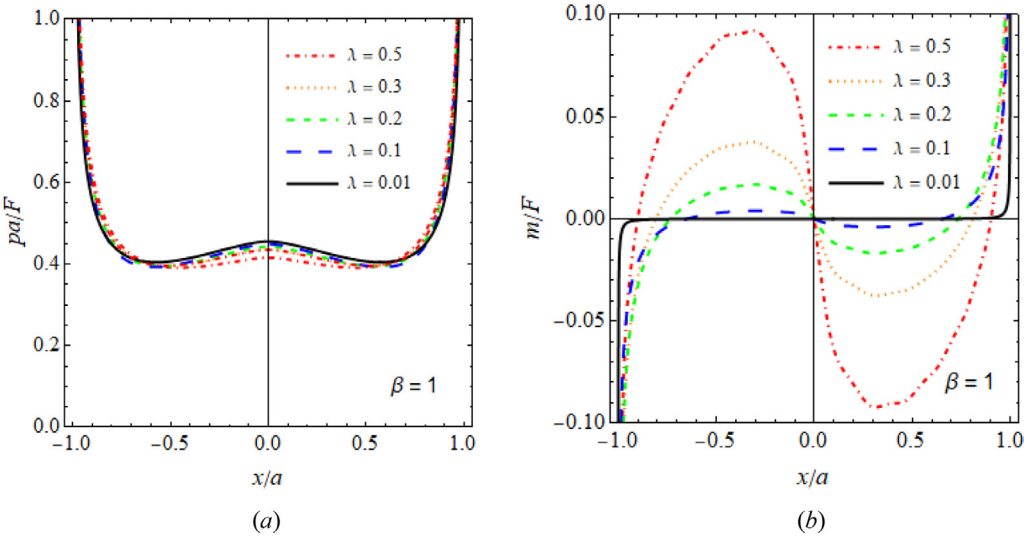

Fig. 12. Distributions of contact pressure (a) and couple stress tractions (b) under the beam due to a point load F applied at $x = 0$, for $\beta = 1$ and $\nu = 0.3$, for some values of the non-dimensional ratio λ, for microstructural boundary conditions of Type III.

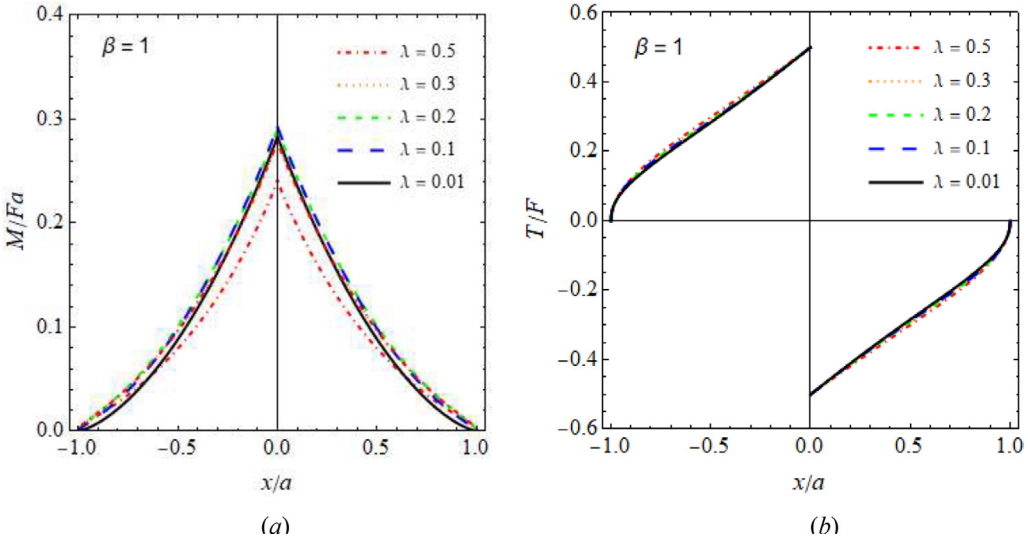

Fig. 13. Distributions of bending moment (a) and shear force (b) along the beam due to a point load F applied at $x = 0$, for $\beta = 1$ and $\nu = 0.3$, for some values of the non-dimensional ratio λ, for microstructural boundary conditions of Type III.

6. Conclusions

In this work, an analytical investigation of the plane problem of a loaded EB beam in full and frictionless contact with a couple stress elastic half-plane is performed. The contact problem was solved by imposing the classical compatibility condition between the slope of the beam and that of the half-plane along the contact region together with an additional microstructural contact condition of three different types. The fundamental solutions for the couple stress half-plane under point force and point couple applied at its surface was used for reducing the problem to one or two integral equations. The unknown contact pressure and couple stress tractions under the beam were expanded in series of Chebyshev polynomials. Both fields were assumed to display square-root singularity at the beam ends, in agreement with the predictions of the asymptotic analysis. The collocation method was then implemented for solving the governing integral equations.

The study allows to evaluate in detail the influence of the micropolar properties of the ground on the bending moment and shear force in the beam, under the action of an arbitrary system of external loads. The classical elastic solution is recovered as the characteristic length becomes vanishing small. Generally, the magnitude of the couple stress tractions is found to increase with the characteristic length. Although its contribution is usually smaller than that of the contact pressure and mainly restricted to the edges of the beam, it may provide a significant influence on the shear force and bending moment along the beam. Therefore, the obtained results show that the couple stress tractions significantly affect the beam internal forces and moments, and size dependent behavior is exhibited when the beam length is comparable to the intrinsic characteristic length scale of the ground.

Overall, the current work analyzes for the first time the role of the moment tractions and, more in general, of the microstructural

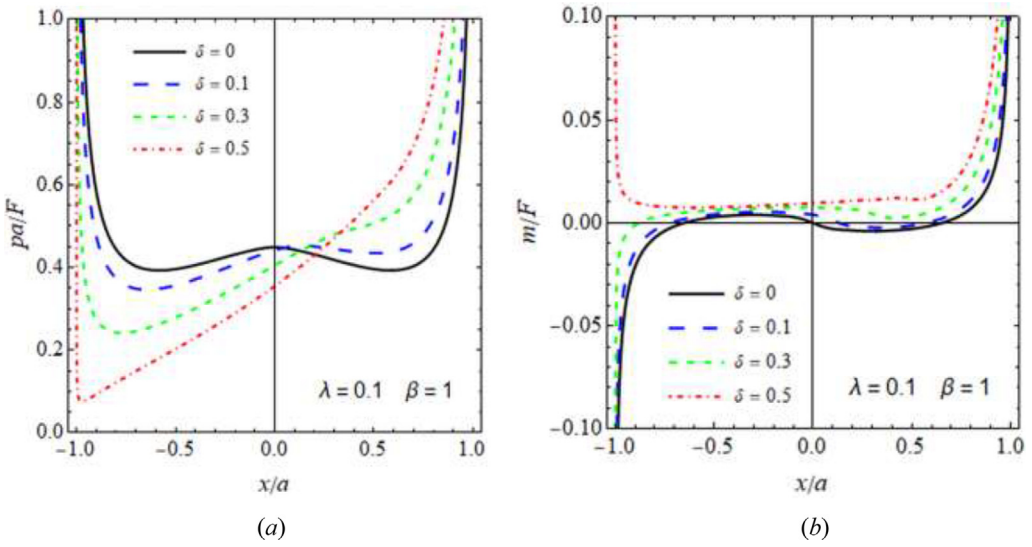

(*a*) (*b*)

Fig. 14. Distributions of contact pressure (*a*) and couple stress tractions (*b*) under the beam due to a point load *F* applied at $x = \delta a$, for $\beta = 1$ and $\nu = 0.3$, for some values of the non-dimensional ratio λ, for microstructural boundary conditions of Type III.

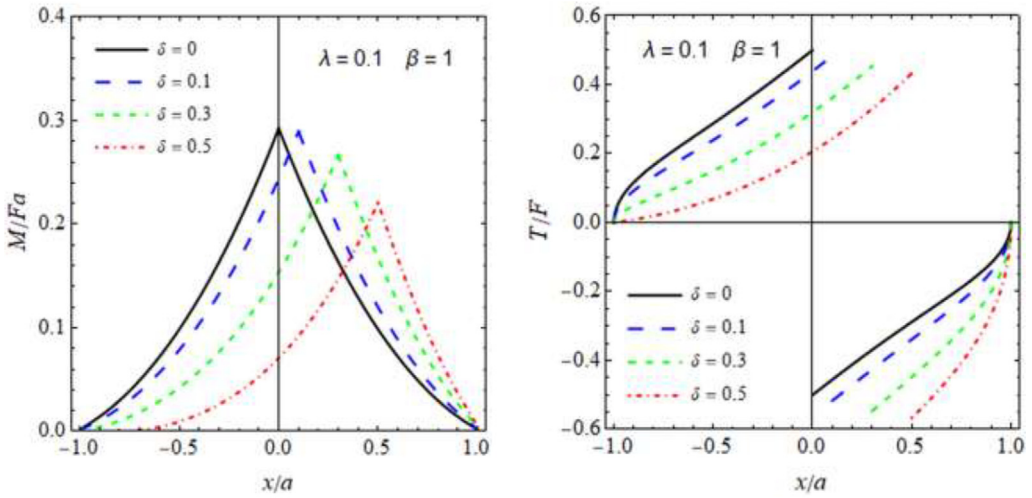

(*a*) (*b*)

Fig. 15. Distributions of bending moment (*a*) and shear force (*b*) along the beam due to a point load *F* applied at $x = \delta a$, for $\beta = 1$, $\lambda = 0.1$ and $\nu = 0.3$, for some values of δ, for microstructural boundary conditions of Type III.

contact conditions on the internal forces of structural members in contact with a microstructured half-plane.

In particular, we showed that the condition of vanishing rotation along the contact zone yields unusual distributions of couple stress tractions and bending moment along the beam, although such an assumption has been considered in some works in the literature. We also think that the assumption of vanishing couple stress tractions may be correct if no rotational energy is transmitted across the interface, and the Type III contact condition, which requires the same macroscopic rotation between the beam and the couple stress substrate, is the most correct one if the elements in contact "lock" together, or form a common "elastic boundary layer". Evidence is provided that accounting for the moment tractions along the contact zone and micropolar behavior of the half-plane yields a significantly different response from the classical elastic solution. Moreover, it is shown that finite values of the intrinsic characteristic length are a prerequisite for non-negligible size effects to appear. In particular, it is found that size effects can be significant in the range of internal length values that is relevant for a wide range of commonly-used engineering materials. Moreover, we show that accounting for the micropolar behavior of the ground, but neglecting the moment tractions in the contact region may lead to a substantial underestimation of the bending moment in the beam, in particular for the intermediate range of internal length values.

The most interesting applications concern the case of beam length comparable with the microstructural characteristic length, namely for the values of λ about 0.5 and 1. These results are expected to be significant and useful for engineering applications, specially in the field of micromechanics. We aspire indeed that the provided results may serve as a reference for the design of structural components in contact with heterogeneous and complex

materials, not only at the macroscale, but also at the micro and nanoscale, providing a fundamental basis for the assessment of the proper microstructural contact conditions.

Declaration of Competing Interest

The author declares that he has no known competing financial interests or personal relationships that could have appeared to influence the work reported in this paper.

Acknowledgement

Support from the Italian "Gruppo Nazionale di Fisica Matematica" INdAM-GNFM is gratefully acknowledged. The author is also grateful to Professor Panos Gourgiotis for his valuable comments.

Appendix A. Local displacement, slope and rotation fields due to a concentrated couple

Here, the asymptotic behavior of the vertical displacement and rotation is analyzed near the point of application of the concentrated couple C. The function $w(z)$ defined in (3.8) displays the following behavior at infinity

$$w(z)=\frac{1}{(6-4\nu)(z^2+1)}+O\left(\frac{1}{z^4}\right),\quad \text{as } z\to\infty. \tag{A.1}$$

Then, the introduction of (A.1) in (3.7) allows us to split the vertical displacement into the following two parts

$$u_y^C(x,0)=C\,\frac{1-\nu}{\pi\,\mu\ell}\left\{\frac{1}{6-4\nu}\int_0^\infty\frac{1}{z^2+1}\sin\frac{zx}{\ell}\,dz + \int_0^\infty\left[w(z)-\frac{1}{(6-4\nu)(z^2+1)}\right]\sin\frac{zx}{\ell}\,dz\right\}, \tag{A.2}$$

where the last integral can be easily calculated numerically, since the term within square brackets decays at infinity as z^{-4}, whereas the first integral, which decays at infinity as z^{-2}, can be calculated analytically according to the result (3.723.1) in Gradshteyn and Ryzhik (2007)

$$\int_0^\infty\frac{1}{z^2+1}\sin\frac{zx}{\ell}\,dz=\frac{1}{2}\left[e^{-x/\ell}Ei\left(\frac{x}{\ell}\right)-e^{x/\ell}Ei\left(-\frac{x}{\ell}\right)\right], \tag{A.3}$$

where Ei denotes the exponential integral function (Gradshteyn and Ryzhik, 2007), whose behavior at the origin is given by

$$Ei(x)=\ln|x|+\Gamma+O(x),\quad \text{as } x\to 0, \tag{A.4}$$

where $\Gamma=0.577215\ldots$ is the Euler constant. Therefore, the vertical displacement is null at $x=0$.

According to (3.9) and (A.1), the slope of the half-plane surface can be split into a singular part and a regular part, namely

$$u_{y,x}^C(x,0)=C\,\frac{1-\nu}{\pi\,\mu\ell^2}\left\{\frac{1}{6-4\nu}\int_0^\infty\frac{z\cos(zx/\ell)}{z^2+1}\,dz + \int_0^\infty\left[w(z)-\frac{1}{(6-4\nu)(z^2+1)}\right]z\cos\frac{zx}{\ell}\,dz\right\}. \tag{A.5}$$

Again, the last regular integral can be calculated numerically, whereas the first singular integral is given by result (3.723.5) in Gradshteyn and Ryzhik (2007) as

$$\int_0^\infty\frac{z}{z^2+1}\cos\frac{zx}{\ell}\,dz=-\frac{1}{2}\left[e^{-x/\ell}\,Ei\left(\frac{x}{\ell}\right)+e^{x/\ell}\,Ei\left(-\frac{x}{\ell}\right)\right]. \tag{A.6}$$

Therefore, the slope near the point of application of the couple displays the following singular logarithmic behavior

$$u_{y,x}^C(x,0)=-\frac{C\,(1-\nu)}{\pi\,\mu\ell^2\,(6-4\nu)}\ln\frac{|x|}{\ell},\quad \text{as } x\to 0. \tag{A.7}$$

By using the asymptotic expansion

$$w(z)[(5-4\nu)\,z+\sqrt{1+z^2}]=\frac{z}{z^2+1}+O\left(\frac{1}{z^3}\right),\quad \text{as } z\to\infty, \tag{A.8}$$

the rotation (3.10) also can be split into the sum of a singular part and a regular, namely

$$\omega_z^C(x,0)=\frac{C}{4\pi\,\mu\ell^2}\left\{\int_0^\infty\frac{z\cos(zx/\ell)}{z^2+1}dz + \int_0^\infty\left[(5z-4\nu\,z+\sqrt{1+z^2})\,w(z)-\frac{z}{z^2+1}\right]\cos\frac{zx}{\ell}dz\right\}, \tag{A.9}$$

where the first singular integral is given in (A.6) and the last integral is regular according to (A.8). Therefore, the rotation displays the following singular logarithmic behavior near the point of application of the couple

$$\omega_z^C(x,0)=-\frac{C}{4\pi\,\mu\ell^2}\ln\frac{|x|}{\ell},\quad \text{as } x\to 0. \tag{A.10}$$

Appendix B. Useful integrals involving Chebyshev polynomials

The Chebyshev polynomial of the first kind of order n is defined as:

$$T_n(t)=\cos(n\arccos t), \tag{B.1}$$

where $0\le\arccos t\le\pi$. They form a complete orthogonal set in the interval [-1, 1] with respect to the weight function $(1-t^2)^{-1/2}$, namely:

$$\int_{-1}^{1}\frac{T_n(t)\;T_m(t)}{\sqrt{1-t^2}}\,dt=\begin{cases}\pi/2 & \text{if } n=m\neq 0,\\ \pi & \text{if } n=m=0,\\ 0 & \text{if } n\neq m.\end{cases} \tag{B.2}$$

By using the definition (B.1) and making the substitution $t=\cos\theta$, the following definite integrals can be calculated:

$$\int_{-1}^{1}\frac{T_n(\tau)}{(\xi-\tau)\sqrt{1-\tau^2}}d\tau=-\pi\,U_{n-1}(\xi), \tag{B.3}$$

$$\int_{-1}^{1}\frac{T_n(\tau)}{\sqrt{1-\tau^2}}\sin[\alpha\,(\xi-\tau)]\,d\tau=\pi\,J_n(\alpha)\sin\left(\alpha\xi-\frac{n\pi}{2}\right), \tag{B.4}$$

$$\int_{-1}^{1}\frac{T_n(\tau)}{\sqrt{1-\tau^2}}\cos[\alpha\,(\xi-\tau)]\,d\tau=\pi\,J_n(\alpha)\cos\left(\alpha\xi-\frac{n\pi}{2}\right), \tag{B.5}$$

where the result (B.3) is given in Erdogan and Gupta (1972) and the integrals (B.4) and (B.5) can be calculated by using results (3.715.13) and (3.715.18) in Gradshteyn and Ryzhik (2007), and U_n is the Chebyshev polynomial of the second kind of order n, which is defined as:

$$U_n(t)=\frac{\sin[(n+1)\arccos t]}{\sin(\arccos t)}. \tag{B.6}$$

Appendix C. Calculation of definite integrals (4.8)

Let us define

$$C_n^{(m)}(\xi)=\int_{-1}^{\xi}\frac{T_n(\tau)}{\sqrt{1-\tau^2}}\,\tau^m d\tau,\quad \text{for } m=0,1,2;\;\; n\geqslant 0. \tag{C.1}$$

Then, making the substitution $\tau=\cos\theta$, the definite integrals (C.1) can be calculated in closed-form:

$$C_n^{(0)}(\xi)=\int_{\arccos\xi}^{\pi}\cos n\theta\,d\theta=\begin{cases}-\sqrt{1-\xi^2}\,U_{n-1}(\xi)/n, & \text{if } n\neq 0,\\ \pi-\arccos\,\xi, & \text{if } n=0,\end{cases} \tag{C.2}$$

$$C_n^{(1)}(\xi) = \int_{\arccos\ \xi}^{\pi} \cos n\theta \cos\theta\, d\theta = \begin{cases} -\frac{\sqrt{1-\xi^2}}{2}\left[\frac{U_n(\xi)}{n+1} + \frac{U_{n-2}(\xi)}{n-1}\right], & \text{if } n \neq 1, \\ \frac{1}{2}\left[\pi - \arccos\ \xi - \xi\sqrt{1-\xi^2}\right], & \text{if } n = 1, \end{cases} \tag{C.3}$$

$$C_n^{(2)}(\xi) = \int_{\arccos\ \xi}^{\pi} \cos n\theta\, (\cos\ \theta)^2\, d\theta = \begin{cases} \sqrt{1-\xi^2}\ \frac{2n\xi\ T_n(\xi) + (2-n^2\xi^2)\ U_{n-1}(\xi)}{n\ (n^2-4)}, & \text{if } n \neq 0,\ 2, \\ (\pi - \arccos\ \xi - \xi\sqrt{1-\xi^2})/2, & \text{if } n = 0, \\ [\pi - \arccos\ \xi - \xi\,(1+2\xi^2)\ \sqrt{1-\xi^2}]/4, & \text{if } n = 2. \end{cases} \tag{C.4}$$

Therefore, the definite integrals (4.8) are given by

$$A_n(\xi) = \xi^2 C_n^{(0)}(\xi) - 2\xi\, C_n^{(1)}(\xi) + C_n^{(2)}(\xi),$$

$$B_n(\xi) = \xi\, C_n^{(0)}(\xi) - C_n^{(1)}(\xi). \tag{C.5}$$

References

Barber, J.R., 2018. Contact mechanics. Solid Mechanics and Its Applications Vol. 250. Springer.

Erdogan, F., Gupta, G.D., 1972. On the numerical solution of singular integral equations. Q. Appl. Math. 29 (4), 525–534.

Erdogan, F., 1969. Approximate solutions of systems of singular integral equations. SIAM J. Appl. Mathem. 17 (6), 1041–1059.

Eremeyev V.A., Skrzat A., Stachowicz F., 2016a. On Finite Element Computations of Contact Problems in Micropolar Elasticity. Adv. Mater. Sci. Eng., 2016, Article ID 9675604.

Eremeyev V.A., Skrzat A., Vinakurava A., 2016b. Application of the micropolar theory to the strength analysis of bioceramic materials for bone reconstruction. Strength Mater., 48(4), 573–582, 2016.

Eremeyev, V.A., Skrzat, A., Stachowicz, F., 2017. Linear micropolar elasticity analysis of stresses in bones under static loads. Strength Mater. 49 (4), 575–585.

Falope, F.O., Lanzoni, L., Radi, E., 2020. Buckling of a Timoshenko beam bonded to an elastic half-plane: effects of sharp and smooth beam edges. Int. J. Solids Struct. 185-186, 222–239.

Gourgiotis, P.A., Georgiadis, H.G., 2011. The problem of sharp notch in couple-stress elasticity. Int. J. Solids Struct. 48 (19), 2630–2641.

Gourgiotis, P.A., Zisis, T.h., 2016. Two-dimensional indentation of microstructure solids characterized by couple-stress elasticity. J. Strain Analysis Eng. Design 51, 1–14.

Gourgiotis, P.A., Zisis, T.h., Baxevanakis, K.P., 2016. Analysis of the tilted flat punch in couple-stress elasticity. Int. J. Solids Struct. 85-86, 34–43.

Gradshteyn, I.S., Ryzhik, I.M., 2007. Table of Integrals, Series, and Products. Elsevier.

Karuriya, A.N., Bhandakkar, T.K., 2017. Plane strain indentation on finite thickness bonded layer in couple stress elasticity. Int. J. Solids Struct. 108, 275–288.

Koiter, W.T., 1964. Couple-stresses in the theory of elasticity, I and II. Proc. Kon. Nederl. Akad. Wetensch (B) 67, 17–44.

Lanzoni, L., Radi, E., 2016. A loaded Timoshenko beam bonded to an elastic half plane. Int. J. Solids Struct. 92 (1), 76–90.

Lewandowski-Szewczyk, M.J., Stupkiewicz, S., 2020. Non-standard contact conditions in generalized continua: microblock contact model for a Cosserat body. Int. J. Solids Struct. 202, 881–894.

Liu, S., Su, W., 2009. Effective couple-stress continuum model of cellular solids and size effects analysis. Int. J. Solids Struct. 46 (14-15), 2787–2799.

Mindlin, R.D., 1963. Influence of couple-stresses on stress concentrations. Exp. Mech. 3 (1), 1–7.

Mindlin, R.D., Tiersten, H.F., 1962. Effects of couple-stresses in linear elasticity. Arch. Ration. Mech. Anal. 11 (1), 415–448.

Morini, L., Piccolroaz, A., Mishuris, G., Radi, E., 2013. On fracture criteria for dynamic crack propagation in elastic materials with couple stresses. Int. J. Eng. Sci. 71, 45–61.

Nobili, A., Radi, E., Vellender, A., 2019. Diffraction of antiplane shear waves and stress concentration in a cracked couple stress elastic material with micro inertia. J. Mech. Phys. Solids 124, 663–680.

Piccolroaz, A., Mishuris, G., Radi, E., 2012. Mode III interfacial crack in the presence of couple-stress elastic materials. Eng. Fract. Mech. 80, 60–71.

Radi, E., 2007. Effects of characteristic material lengths on mode III crack propagation in couple stress elastic-plastic materials. Int. J. Plast. 23 (8), 1439–1456.

Radi, E., 2008. On the effects of the characteristic lengths in bending and torsion on Mode III crack in couple stress elasticity. Int. J. Solids Struct. 45 (10), 3033–3058.

Sackfield, A., Hills, D.A., Nowell, D., 2013. Mechanics of Elastic Contacts. Elsevier.

Shield, T.W., Kim, K.S., 1992. Beam theory models for thin film segments cohesively bonded to an elastic half space. Int. J. Solids Struct. 29 (9), 1085–1103.

Song, H.X., Ke, L.L., Wang, Y.S., 2017. Sliding frictional contact analysis of an elastic solid with couple stresses. Int. J. Mech. Sci. 133, 804–816.

Toupin, R.A., 1962. Perfectly elastic materials with couple stresses. Arch. Ration. Mech. Anal. 11 (1), 385–414.

Weitsman, Y., 1965. Couple-stress effects on stress concentration around a cylindrical inclusion in a field of uniaxial tension. J. Appl. Mech., 424–428.

Zhang, H.W., Wang, H., Wriggers, P., Schrefler, B.A., 2005. A finite element model for contact analysis of multiple Cosserat bodies. Comput. Mech. 36 (6), 444–458.

Zisis, T.h., Gourgiotis, P.A., Baxevanakis, K.P., Georgiadis, H.G., 2014. Some basic contact problems in couple stress elasticity. Int. J. Solids Struct. 51 (11-12), 2084–2095.

Zisis, T.h., Gourgiotis, P.A., Georgiadis, H.G., 2018. Contact mechanics in the framework of couple stress elasticity. In: Altenbach, H. (Ed.), Generalized Models and Non-Classical Approaches in Complex Materials 2, Advanced Structured Materials, 90, Chapter 14. Springer, pp. 279–306.